



CHORUS

This is the accepted manuscript made available via CHORUS. The article has been published as:

Dynamics of pattern-loaded fermions in bichromatic optical lattices

Matthew D. Reichl and Erich J. Mueller

Phys. Rev. A **93**, 031601 — Published 11 March 2016

DOI: [10.1103/PhysRevA.93.031601](https://doi.org/10.1103/PhysRevA.93.031601)

Dynamics of pattern-loaded fermions in bichromatic optical lattices

Matthew D. Reichl and Erich J. Mueller

Laboratory of Atomic and Solid State Physics, Cornell University, Ithaca, New York 14853, USA

Motivated by experiments in Munich (M. Schreiber et. al. Science **349**, 842), we study the dynamics of interacting fermions initially prepared in charge density wave states in one-dimensional bichromatic optical lattices. The experiment sees a marked lack of thermalization, which has been taken as evidence for an interacting generalization of Anderson localization, dubbed “many-body localization”. We model the experiments using an interacting Aubry-Andre model and develop a computationally efficient low-density cluster expansion to calculate the even-odd density imbalance as a function of interaction strength and potential strength. Our calculations agree with the experimental results and shed light on the phenomena. We also explore a two-dimensional generalization. The cluster expansion method we develop should have broad applicability to similar problems in non-equilibrium quantum physics.

PACS numbers: 72.15.Rn, 37.10.Jk, 67.85.-d

Introduction - An important challenge in many-body physics is to understand how interactions and disorder influence the transport properties of an electron gas. The non-interacting disordered problem was largely solved by Anderson [1, 2]. By studying the expansion dynamics of wave packets of weakly interacting atoms, cold atom experiments have found evidence for Anderson localization in 1D [3] and 3D [4, 5] random speckled potentials and in 1D quasi random optical superlattices [6]. More recently, attention has turned to the interacting problem [7–25]. Schreiber et. al [26] devised an ingenious experiment to

test these ideas. Here we model that experiment.

The experiment in Ref. [26] uses lasers to create a one-dimensional lattice with a weak periodic superlattice that is incommensurate with the main lattice (see the inset in Fig. 1). The resulting quasi-periodic potential shares features with a disordered one. For example, when the potential is sufficiently strong, all single particle states are localized. The experimentalists load interacting spin-1/2 fermions into some of the odd sites of the lattice, leaving the even sites empty. Some odd sites are doubly occupied. The atoms hop and interact for time t . The experimentalists measure the sublattice imbalance $I(t)$

$$I(t) = \frac{N_{\text{odd}} - N_{\text{even}}}{N_{\text{odd}} + N_{\text{even}}} \quad (1)$$

where $N_{\text{odd/even}}$ is the number of fermions on odd/even sites at time t . In a localized phase, the atoms do not travel far from their initial position, and have a relatively high probability of being found at their starting point. Consequently in such a phase, one expects $I(t)$ to be non-zero at long times. Conversely, in a delocalized phase, one might expect $I(t)$ to decay to zero at long times. The experiment explores the long time behavior of I as a function of superlattice strength and the interaction strength. The initial configuration of fermions on odd sites is random and the measurements are the result of ensemble averages over initial states. The experimentalists find two phases: one in which I decays to zero, the other in which it is finite. The boundary appears to depend on the interactions in a non-monotonic manner.

In this paper we model the experiment, addressing the fundamental question of the interplay of incommensurate potentials and interactions. We develop a low-density cluster expansion which expresses the ensemble averaged imbalance as the sum of terms which involve only single-particle and two-particle dynamics. Using this computationally efficient approximation, we numerically calculate the long time imbalance as a function of interaction strength and superlattice strength. Our calculations reproduce the experimental results and provide insight into localization in the interacting system. We also extend our

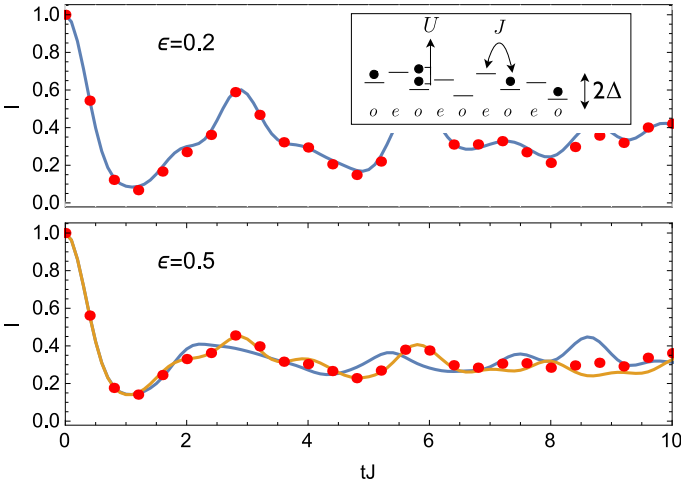


FIG. 1: (Color online) Imbalance $I = \frac{N_{\text{odd}} - N_{\text{even}}}{N_{\text{odd}} + N_{\text{even}}}$ vs time t , measured in units of the nearest-neighbor hopping strength J for fermions in an incommensurate superlattice of strength Δ . $N_{\text{odd/even}}$ is the number of fermions on odd/even sites. The inset shows the geometry. At time $t = 0$, $I = 1$. The dark (blue) curves show the result of keeping the first two terms in the cluster expansion in Eq. (6) for 20 sites. The light (orange) curve shows the result of including three-particle terms in the cluster expansion. Red dots correspond to a time-dependent DMRG simulation. Here $\Delta = 3J$, $U = 3J$, the superlattice period $\beta^{-1} = (0.721)^{-1}$ and the superlattice phase $\phi = 0$. The density is $\epsilon = 0.2$ in the top graph and $\epsilon = 0.5$ in the bottom graph.

method to the case of a two dimensional lattice with an incommensurate superlattice in only one direction. The extra transverse degrees of freedom give kinetic pathways for equilibration; we calculate the consequences.

Model and Methods - We model the atomic dynamics via the interacting Aubry-Andre model, given by the Hamiltonian [14, 27]

$$H = -J \sum_{i,\sigma} \left(c_{i,\sigma}^\dagger c_{i+1,\sigma} + \text{h.c.} \right) + \Delta \sum_{i,\sigma} \cos(2\pi\beta i + \phi) c_{i,\sigma}^\dagger c_{i,\sigma} + U \sum_i n_{i,\uparrow} n_{i,\downarrow} \quad (2)$$

The first term describes nearest neighbor tunneling with strength J while the second term describes a periodic superlattice potential of strength Δ . For nearly all irrational values of β , this potential functions as quasirandom disorder which localizes all single particle states for sufficiently large superlattice strength ($\Delta/J > 2$) [27]. In this regime, and for infinitely large systems, the single particle states are localized with a localization length $\lambda = (2 \log \frac{\Delta}{2J})^{-1}$, independent of β [27, 28]. If $\beta = p/q$ is rational, the eigenstates are extended Bloch waves with period q . For large Δ and large q , the wavefunction in each unit cell is sharply peaked, and locally the eigenstates are similar to the irrational case.

The localization transition is reflected in the observable $I(t)$, which for typical irrational β and $U = 0$ relaxes to 0 for $\Delta/J < 2$ but remains finite at long times for $\Delta/J > 2$ (see the inset in Fig. 2). We define $I_\infty = I(t \rightarrow \infty)$. Although $I_\infty \rightarrow 0$ as $\Delta/J \rightarrow 2$, the way it vanishes depends strongly on β and is inconsistent with the naive estimate from structureless exponentially localized states $I_{\text{est}} \sim 1/\lambda^2$ (see Ref. [26], supplementary material). The graph of I_∞ vs. β and Δ/J is fractal (see Fig. S1 in the Supplementary Information), as it has different behaviors for rational and irrational β . Despite this complexity, the

long time behavior of I is distinct in the localized and delocalized phase: $I(t)$ captures the localization transition, but also probes features of the single-particle wave functions beyond the localization length.

The third term in Eq. (2) describes on-site interactions of strength U . Here we develop a low-density expansion to calculate the imbalance in the presence of interactions.

We define $\langle I(t) \rangle$ to be the expectation value of the imbalance, averaged over the ensemble of initial states,

$$\langle I(t) \rangle = \frac{1}{Z} \sum_{n=1}^{N_s} \sum_{\{n\}} W(\{n\}) \times \frac{1}{n} \langle \{n\} | \hat{n}_I(t) | \{n\} \rangle \quad (3)$$

Here $\{n\} = \{i_1\sigma_1, i_2\sigma_2, \dots, i_n\sigma_n\}$ labels an n -particle initial state with particles at sites i with spin σ , $\sum_{\{n\}}$ denotes a sum over the i_j 's and σ_j 's, $W(\{n\})$ is the weight of a given n particle state, $Z = \sum_{\{n\}} W(\{n\})$, and $\hat{n}_I(t) = e^{iHt} (\hat{N}_{\text{odd}} - \hat{N}_{\text{even}}) e^{-iHt}$ where $\hat{N}_{\text{odd/even}}$ are the number operators (for both spins) on odd/even sites.

To model the experiment, we take $W(\{n\}) = 0$ if any of the particles are on even sites. We take the initial occupation of each odd site to be an independent random variable, and hence $W(\{n\}) = \epsilon^n (1 - \epsilon)^{N_s - n}$, where N_s is the number of sites. Our method is readily generalized to more sophisticated weights. For instance, as shown in Eq. (S12), we can weight the initial states with separate probabilities for sites with two atoms (doublons) or one atom (singlons) (see also Fig. 3).

With this choice of W , the normalization is $Z = 1 - (1 - \epsilon)^{N_s}$ which approaches 1 in the $N_s \rightarrow \infty$ limit. In that same limit, the mean density (the number of particles per site averaged over the ensemble of initial states) is ϵ .

Substituting our weight function into Eq. (3) yields an expression for the imbalance as a sum of terms involving different numbers of particles:

$$\langle I(t) \rangle = \frac{1}{Z} \left[\epsilon (1 - \epsilon)^{N_s - 1} \sum'_{\{1\}} C_{\{1\}}(t) + \frac{\epsilon^2}{2} (1 - \epsilon)^{N_s - 2} \sum'_{\{2\}} C_{\{2\}}(t) + \frac{\epsilon^3}{3} (1 - \epsilon)^{N_s - 3} \sum'_{\{3\}} C_{\{3\}}(t) + \dots + \frac{\epsilon^{N_s}}{N_s} \sum'_{\{N_s\}} C_{\{N_s\}}(t) \right] \quad (4)$$

where $C_{\{n\}}(t) = \langle \{n\} | \hat{n}_I(t) | \{n\} \rangle$, and the primes on the sums mean they only include odd sites.

We wish to resum this series, taking advantage of the fact that well-separated particles will move independently. Somewhat analogous to cumulants, we define functions $\tilde{C}_{\{n\}}(t)$ via

$$C_{\{n\}}(t) = \tilde{C}_{\{n\}}(t) + \sum_{\{\{1\} \in \{n\}\}} C_{\{1\}}(t) + \sum_{\{\{2\} \in \{n\}\}} \tilde{C}_{\{2\}}(t) + \sum_{\{\{3\} \in \{n\}\}} \tilde{C}_{\{3\}}(t) + \dots + \sum_{\{\{n-1\} \in \{n\}\}} \tilde{C}_{\{n-1\}}(t) \quad (5)$$

where $\sum_{\{\{k\} \in \{n\}\}}$ denotes a sum over all $\binom{n}{k}$ combinations of k site and spin labels in $\{n\}$. We set $\tilde{C}_{\{1\}}(t) = C_{\{1\}}(t)$. These new functions $\tilde{C}_{\{k\}}(t)$ extract

the k -body dynamics from the original functions $C_{\{k\}}(t)$. First instance, the two particle term $\tilde{C}_{\{i_1\sigma_1, i_2\sigma_2\}}(t) = C_{\{i_1\sigma_1, i_2\sigma_2\}}(t) - C_{\{i_1\sigma_1\}}(t) - C_{\{i_2\sigma_2\}}(t)$ is the difference

between a term representing the exact dynamics of two particles with initial positions and spins $i_1\sigma_1$ and $i_2\sigma_2$ and the single particle dynamics of a particle initialized at site i_1 and another particle initialized at site i_2 . In the non-interacting limit $U = 0$, we only have single particle dynamics and $\tilde{C}_{\{k\}}(t) = 0$ for all $k > 1$. In a diagrammatic formulation, \tilde{C} involves only connected diagrams.

Substituting Eq. (5) into Eq. (4), and using the arguments in the Supplementary Information gives

$$\langle I(t) \rangle = \frac{1}{N_s} \sum_{\{1\}} \tilde{C}_{\{1\}}(t) + \frac{\epsilon}{N_s} \sum_{\{2\}} \tilde{C}_{\{2\}}(t) + O(\epsilon^2) \quad (6)$$

in the $N_s \rightarrow \infty$ limit. For our numerical calculations we include the finite size corrections in Eq. (S7).

Equation (6) expresses the n -particle time dependent observable $\langle I(t) \rangle$ explicitly as the sum of 1-particle terms ($\tilde{C}_{\{1\}}(t)$), 2-particle terms ($\tilde{C}_{\{2\}}(t)$), etc. The first sum in Eq. (6) contains N_s terms. The second sum contains $O(N_s^2)$ terms, but when the two particles are farther apart than some length scale ξ , where ξ is the smaller of the one-particle localization length λ and the ballistic length $l = Jt$, the particles are effectively non-interacting and $\tilde{C}_{\{2\}}$ will vanish. Therefore only ξN_s terms contribute to the sum. Similarly, there are only $O(\xi^2 N_s)$ which contribute in the sum over $\tilde{C}_{\{3\}}$ terms.

Each subsequent term in Eq. (6) is intensive and is weighted by a coefficient of the order ϵ^{n-1} (the density exponentiated to the number of particles in the cluster minus 1). This cluster expansion is a non-equilibrium analogue to the virial expansion in statistical physics [29]. When the localization length is greater than the system size ($\lambda > N_s$) the series is only guaranteed to converge for short times $l = Jt \lesssim 1/\epsilon$. Therefore, for calculations of the long-time behavior of the imbalance, we focus our attention on the localized regime $\Delta/J > 2$.

For most of the results in this paper we only keep the first two terms in Eq. (6). Remarkably, this approximation, which only involves calculating the dynamics of one or two particles, shows all the features seen in the experiments of Ref. [26].

Numerical Results - Figure 1 shows typical $\langle I(t) \rangle$ for interacting fermions in the localized regime. The solid blue curves show calculations using the first two terms in the cluster expansion in Eq. (6). The imbalance initially has a value $I(t=0) = 1$, reflecting the fact that the initial states have particles localized only on odd sites. At long times, the imbalance saturates to a non-zero value with small fluctuations about the mean. For comparison, the red dots show calculations using time-dependent density matrix renormalization group (t-DMRG) [30, 31]. For the DMRG calculations, we average over 100 initial states drawn from the probability distribution $W(\{n\})$. The cluster expansion and the t-DMRG show excellent agreement at the smaller density $\epsilon = 0.2$. At the larger density $\epsilon = 0.5$ there is some small quantitative disagreement, but the average long-time imbalance is nearly identical for the two approaches. As a test of the conver-

gence of the cluster expansion, we have also computed the contribution from three-particle terms (orange curve in Fig. 1). Including these terms gives small corrections to the two-particle calculation and yields better agreement with t-DMRG.

Figure 2 shows the long time imbalance I_∞ as a function of interaction strength for a series of superlattice strengths. We compute $\langle I(t) \rangle_{\text{init}}$ by numerically evaluating the first two terms of Eq. (6) at a density $\epsilon = 0.2$. Each data point in Fig. 2 represents $\langle I(t) \rangle$ averaged over the times $200 < tJ < 500$ and averaged over twelve values of the superlattice potential phase ϕ evenly spaced in the range $[0, \pi]$. All simulations were performed on a lattice with 20 sites using open boundary conditions. We have explicitly verified that finite size effects are negligible; the system size was chosen for numerical convenience.

Each curve is symmetric under $U \rightarrow -U$. As pointed out in Ref. [32] this symmetry is expected for time-reversal invariant operators such as $I(t)$, as long as the initial states are localized in space. For $|U/J| \lesssim 2\Delta$, interactions cause some 2-particle scattering states to become less localized than 1-particle states, and the long time imbalance decreases with increasing interaction strength. For larger interactions, the imbalance begins to increase again and produces a ‘‘W’’ shape consistent with the re-entrant behavior predicted for similar systems [33]. The ‘‘W’’ is most pronounced for $\Delta/J \approx 3$.

At large interaction strengths, up-spin and down-spin particles initially localized at the same site (doublons) become bound and have a reduced effective tunneling rate $J_{\text{eff}} \approx J^2/U$ [8, 12]. The contribution to I_∞ from these doublons causes the long time imbalance at large interaction strengths to become greater than the long-time imbalance at $U = 0$.

We further explore the contribution of doublons to I_∞ by giving doublons and singlons separate weights in our average over initial states (see Eq. (S12)). We let ϵ be the total density of particles and η the density of doublons. Fig. 3 shows I_∞ as a function of U/J at $\Delta/J = 3$ for three different values of η/ϵ in the initial states of the system: 0 ($\epsilon = 0.5$), 0.23 ($\epsilon = 0.57$), and 0.5 ($\epsilon = 0.67$) for the bottom (blue), middle (orange), top (green) graphs, respectively. All other parameters are the same as in Figure 2. In the case where there are no doublons $I_\infty(U/J = 0) = I_\infty(U/J \rightarrow \infty)$. This is a reflection of the fact that the dynamics of singlons in the hard core $U/J \rightarrow \infty$ limit is identical to the dynamics of free spinless fermions [26]. As more doublons are added to the system, I_∞ at large U/J increases, as expected from the reduced tunneling rate of bound pairs. The blue and orange points in Fig. 3 show corresponding experimental results from Ref. [26], where the doublon density was controlled by varying the loading protocol.

We chose η and ϵ to best match the experimental data, finding excellent agreement. Our best-fit value of η is somewhat smaller than estimates in Ref. [26]. Similar discrepancies were seen in DMRG calculations [26].

Motivated by more recent experiments [34], and as a

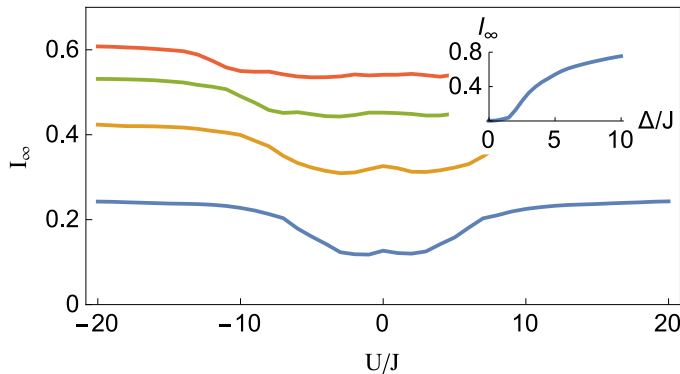


FIG. 2: (Color online) Long time density imbalance I_∞ as a function of interaction strength U/J for a one-dimensional lattice with 20 sites at density $\epsilon = 0.2$. The superlattice period is $\beta^{-1} = (0.721)^{-1}$ in units of the lattice spacing. The different curves correspond to different superlattice strengths: $\Delta/J = 2, 3, 4, 5$ (from bottom to top). The inset shows I as a function of superlattice strength for $U/J = 0$.

further demonstration of our cluster method approach, we have extended our calculations to two-dimensional lattices. We consider a two-dimensional Hamiltonian with a one-dimensional superlattice potential $V = \Delta \cos(2\pi\beta i_x + \phi)$. As before, we take J to be the hopping in the x-direction and J_y the hopping in the y-direction. In this case we average over initial states where atoms are localized on odd sites in the x-direction and are in $k_y = 0$ momentum eigenstates in the y-direction. This choice of initial states, which requires periodic boundary conditions in the y-direction, was chosen purely for numerical simplicity; we expect no qualitative changes if we initialize with spatially localized states and use open boundary conditions in the y-direction. We once again use Eq. (6) including only one-particle and two-particle terms to compute the even-odd imbalance in the x-direction.

Because the eigenstates are inherently delocalized in this situation, we only expect our cluster expansion to be accurate for short times. Fig. 4 shows the imbalance I in the x-direction, averaged over times between $t = 5/J$ and $t = 10/J$ as a function of U/J . These simulations were performed on a lattice with 10×10 sites. Scattering in the y-direction (transverse to the superlattice potential) allows for the density imbalance to relax to smaller values, and I becomes suppressed as J_y is increased. Similar results are observed in Ref. [34].

Conclusion - In this paper we have applied a new cluster expansion method to simulate experiments [26] which studied the non-equilibrium dynamics of fermions pattern-loaded in quasi-disordered one-dimensional lattices. Our calculations, which involve keeping the first two terms in the cluster expansion and account for only single particle and two particle dynamics, reproduce all experimental features of the long-time density imbalance between even and odd sites, and agree quantitatively

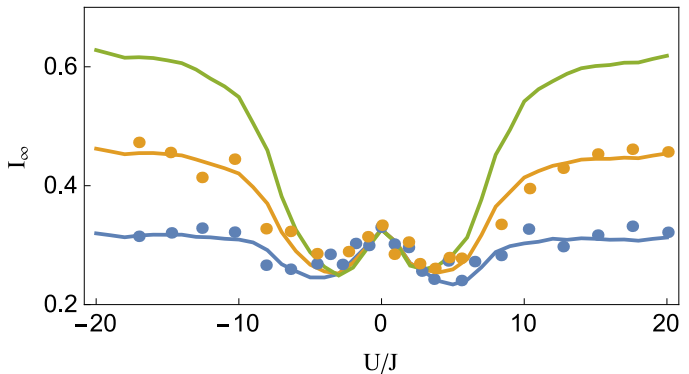


FIG. 3: (Color online) Long time density imbalance I_∞ as a function of interaction strength U/J for a one-dimensional lattice at superlattice strength $\Delta/J = 3$. The different curves show calculations using a cluster expansion on a 20 site lattice with different densities η of doublons in the ensemble of initial states: The bottom (blue), middle (orange), and top (green) curves correspond to a ratio of doublons to particles of $\eta/\epsilon = 0, 0.23, 0.5$, respectively. The blue and orange points are experimental measurements for a small doublon fraction ($\eta/\epsilon \approx 0.08$) and larger doublon fraction ($\eta/\epsilon \approx 0.5$), from Fig. 6 of Ref. [26], courtesy of Ulrich Schneider.

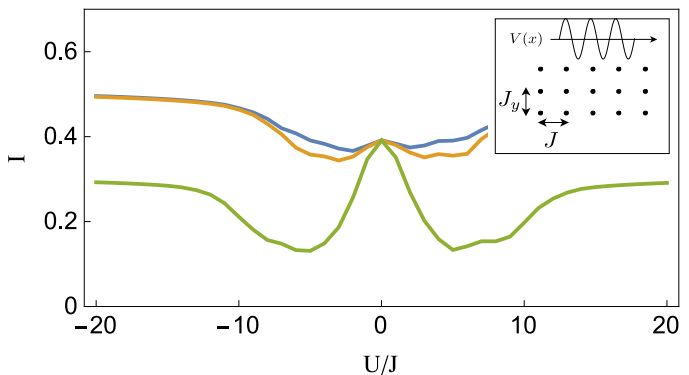


FIG. 4: (Color online) Density imbalance I averaged over time from $t = 5/J$ to $t = 10/J$ as a function of interaction strength U/J for a two-dimensional lattice with 10×10 sites at superlattice strength $\Delta/J = 3.0$ and density $\epsilon = 0.2$. The superlattice potential is only one-dimensional: $V(i_x, i_y) = \Delta \cos(2\pi\beta i_x + \phi)$. $J_y/J = 0, 0.1, 1$ for the top, middle, and bottom (blue, orange, green) curves, respectively. The inset shows a diagram of the setup.

with simulations using t-DMRG. We have also extended our calculations to two-dimensional lattices, finding that the density imbalance is suppressed when adding hopping in the direction transverse to the superlattice potential.

Although principally designed to calculate the experimental observable, this cluster approach also gives some insight into many-body localization. For example we have shown that time dynamics of the many-body wave function in the localized phase can be written as a sum

of 1-body, 2-body, ..., n-body terms. In the dilute limit, the dynamics are dominated by few-particle physics, a feature which was not previously recognized.

Our cluster approach can be also used to explicitly construct the local integrals of motion which underly the phenomenology of the many-body localized phase [15, 17, 35, 36]. As detailed below, we use the solution to the j -body problem to construct fermionic creation operators $a_{n\sigma}^{\dagger(j)}$ where $\{a_{n\sigma}^{(j)}, a_{m\tau}^{\dagger(j)}\} = \delta_{mn}\delta_{\tau\sigma}$. Our operators have the property that in the i -particle subspace, all of the $a_{n\sigma}^{\dagger(j)}$ are equivalent for $j \geq i$: $a_{n\sigma}^{\dagger(i)}P_i = a_{n\sigma}^{\dagger(j)}P_i$ where P_i projects into the i particle subspace. Our conserved quantities are manifest in the requirement

$$[a_{n\sigma}^{\dagger(i)}a_{n\sigma}^{(i)}, P_i H P_i] = 0 \quad (7)$$

If the $a_{n\sigma}^{\dagger(i)}$ are ‘‘local’’, we thereby complete the construction.

We take $a_{n\sigma}^{\dagger(1)}$ to create the single-particle eigenstate with spin σ and energy ϵ_n ; suppressing the spin indices $|n\rangle = a_n^{\dagger(1)}|\text{vac}\rangle$. This operator is local if these eigenstates are localized. Trivially, Eq. (7) is satisfied.

Next we construct

$$a_{n\sigma}^{\dagger(2)} = a_{n\sigma}^{\dagger(1)} + \sum_{\tau\tau'\tau''}^{jkl} \Gamma_{\tau\tau'\tau''}^{n\sigma} a_{j\tau}^{\dagger(1)} a_{k\tau'}^{\dagger(1)} a_{n\tau''}^{(1)} \quad (8)$$

so that $a_{n\sigma}^{\dagger(2)}P_1 = a_{n\sigma}^{\dagger(1)}P_1$. We can always choose the Γ 's such that $|n\sigma, m\tau\rangle = a_{n\sigma}^{\dagger(2)}a_{m\tau}^{\dagger(2)}|\text{vac}\rangle$ is an eigenstate of H with energy $E_{mn}^{\sigma\tau}$. Neglecting the spin indices

$$\Gamma_{jkl}^n = (\langle j| \otimes \langle k|) |nl\rangle - \delta_{jn}\delta_{kl} \quad (9)$$

There are as many ways of doing this as there are ways of assigning the indices to the 2-particle states. We choose the indices to maximize the overlap $(\langle n| \otimes \langle m|) |nl\rangle$. If the two-particle states and one-particle states are localized, then $a_{n\sigma}^{\dagger(2)}$ will be localized. Eq. (7) is clearly satisfied. Constructing the higher order operators follows the same procedure.

To connect with the existing literature [15, 17, 35, 36], we note that this construction yields a Hamiltonian of the form

$$H = \sum_{n\sigma} \epsilon_n \tilde{n}_{n\sigma} + \sum_{\substack{nm \\ \sigma\sigma'}} U_{nm}^{(2)} \tilde{n}_{n\sigma} \tilde{n}_{m\sigma'} + \dots \quad (10)$$

where $\tilde{n}_{n\sigma} = \lim_{j \rightarrow \infty} a_{n\sigma}^{\dagger(j)} a_{n\sigma}^{(j)}$. The coefficients are local, meaning $U_{i_1 i_2 \dots i_k}^{(k)} \sim \exp(-\max|i_\alpha - i_\beta|/\xi_k)$. They can be expressed in terms of the eigenvalues of the k -body problem; for example $U_{nm}^{(2)} = E_{mn}^{\sigma\sigma'} - \epsilon_n - \epsilon_m$. The Supplementary Information shows a graph of this quantity for typical parameters, illustrating the exponential decay.

Acknowledgements- We acknowledge support from ARO-MURI Non-equilibrium Many-body Dynamics grant (W911NF-14-1-0003). We thank Mark Fischer for discussions, and Ulrich Schneider for sharing the experimental data.

-
- [1] P. W. Anderson, Physical review **109**, 1492 (1958).
[2] E. Abrahams, P. Anderson, D. Licciardello, and T. Ramakrishnan, Physical Review Letters **42**, 673 (1979).
[3] J. Billy, V. Josse, Z. Zuo, A. Bernard, B. Hambrecht, P. Lugan, D. Clément, L. Sanchez-Palencia, P. Bouyer, and A. Aspect, Nature **453**, 891 (2008).
[4] S. Kondov, W. McGehee, J. Zirbel, and B. DeMarco, Science **334**, 66 (2011).
[5] F. Jendrzejewski, A. Bernard, K. Mueller, P. Cheinet, V. Josse, M. Piraud, L. Pezzé, L. Sanchez-Palencia, A. Aspect, and P. Bouyer, Nature Physics **8**, 398 (2012).
[6] G. Roati, C. D'Errico, L. Fallani, M. Fattori, C. Fort, M. Zaccanti, G. Modugno, M. Modugno, and M. Inguscio, Nature **453**, 895 (2008).
[7] D. Shepelyansky, Physical Review B **54**, 14896 (1996).
[8] A. Borelli, J. Bellissard, P. Jacquod, and D. L. Shepelyansky, Physical review letters **77**, 4752 (1996).
[9] A. Eilmes, U. Grimm, R. A. Römer, and M. Schreiber, The European Physical Journal B-Condensed Matter and Complex Systems **8**, 547 (1999).
[10] I. Gornyi, A. Mirlin, and D. Polyakov, Physical review letters **95**, 206603 (2005).
[11] D. Basko, I. Aleiner, and B. Altshuler, Annals of physics **321**, 1126 (2006).
[12] G. Dufour and G. Orso, Physical review letters **109**, 155306 (2012).
[13] M. Tezuka and A. M. García-García, Physical Review A **85**, 031602 (2012).
[14] S. Iyer, V. Oganesyan, G. Refael, and D. A. Huse, Physical Review B **87**, 134202 (2013).
[15] M. Serbyn, Z. Papić, and D. A. Abanin, Physical review letters **111**, 127201 (2013).
[16] M. Serbyn, Z. Papić, and D. A. Abanin, Physical Review B **90**, 174302 (2014).
[17] D. A. Huse, R. Nandkishore, and V. Oganesyan, Physical Review B **90**, 174202 (2014).
[18] R. Vosk, D. A. Huse, and E. Altman, arXiv preprint arXiv:1412.3117 (2014).
[19] E. Altman and R. Vosk, Annu. Rev. Condens. Matter Phys. **6**, 383 (2015).
[20] X. Li, S. Ganeshan, J. Pixley, and S. D. Sarma, arXiv preprint arXiv:1504.00016 (2015).
[21] R. Modak and S. Mukerjee, arXiv preprint arXiv:1503.07620 (2015).
[22] Y. Wang, H. Hu, and S. Chen, arXiv preprint arXiv:1505.06343 (2015).
[23] R. Nandkishore and D. A. Huse, Annual Review of Condensed Matter Physics **6**, 15 (2014).

- [24] J. Eisert, M. Friesdorf, and C. Gogolin, *Nature Physics* **11**, 124 (2015).
- [25] T. Devakul and R. R. Singh, *Physical Review Letters* **115**, 187201 (2015).
- [26] M. Schreiber, S. S. Hodgman, P. Bordia, H. P. Lüschen, M. H. Fischer, R. Vosk, E. Altman, U. Schneider, and I. Bloch, *Science* **349**, 842 (2015).
- [27] S. Aubry and G. André, *Ann. Israel Phys. Soc* **3**, 18 (1980).
- [28] J. Sokoloff, *Physics Reports* **126**, 189 (1985).
- [29] M. Kardar, *Statistical physics of particles* (Cambridge University Press, 2007).
- [30] S. R. White, *Physical Review B* **48**, 10345 (1993).
- [31] S. R. White and A. E. Feiguin, *Physical review letters* **93**, 076401 (2004).
- [32] U. Schneider, L. Hackermüller, J. P. Ronzheimer, S. Will, S. Braun, T. Best, I. Bloch, E. Demler, S. Mandt, D. Rasch, et al., *Nature Physics* **8**, 213 (2012).
- [33] V. Michal, I. Aleiner, B. Altshuler, and G. Shlyapnikov, *arXiv preprint arXiv:1502.00282* (2015).
- [34] P. Bordia, H. P. Lüschen, S. S. Hodgman, M. Schreiber, I. Bloch, and U. Schneider, *arXiv preprint arXiv:1509.00478* (2015).
- [35] A. Chandran, I. H. Kim, G. Vidal, and D. A. Abanin, *Physical Review B* **91**, 085425 (2015).
- [36] V. Ros, M. Mueller, and A. Scardicchio, *Nuclear Physics B* **891**, 420 (2015).